Catalysis Today 159 (2011) 144–149

Contents lists available at ScienceDirect

Catalysis Today

journal homepage: www.elsevier.com/locate/cattod

Infrared imaging tool for screening catalyst effect on hydrogen storing thin film libraries

Roger Domènech-Ferrer[a,1], Javier Rodríguez-Viejo[a,b], Gemma Garcia[a,*]

[a] Group of Nanomaterials and Microsystems – GNaM, Physics Department – Universitat Autònoma de Barcelona, Campus UAB – Torre C3-222, 08193 Bellaterra, Barcelona, Spain
[b] MATGAS Research Centre, Campus UAB, 08193 Bellaterra, Spain

ARTICLE INFO

Article history:
Available online 30 October 2010

Keywords:
Metal hydrides
Thin film libraries
Infrared thermography
MgAl
MgFeCu

ABSTRACT

Catalysts and in a larger meaning reaction promoters, are becoming a key partner of metal hydrides and compounds in hydrogen storing systems, largely influencing its kinetics and synthesis process. High-throughput screening techniques provide a unique solution to study in a short period of time the properties and potentialities of large amounts of metal alloys/catalysts combinations for the development of large capacity hydrogen storing hydrides.

In this work, we present preliminary results using the infrared thermography technique as a cheap and simple combinatorial screening tool for compositional effect studies. Hydrogen sorption of combinatorial magnesium-based (MgAl and MgFeCu) libraries, synthesized using vapor phase growth techniques, have been characterized using the infrared imaging and effects of adding Al, Cu and Fe are discussed and compared with literature data.

1. Introduction

Since 1997 when Bogdanovich and Schvickardi [1] observed the reversible two step gas reaction in $NaAlH_4$ when doped with $TiCl_3$, catalysts have become a key partner of metal and complex hydrides in the study of hydrogen sorbing systems, largely influencing its reaction kinetics but mainly its synthesis procedure as otherwise non stable compounds can be prepared. The need for materials with high storing densities along with large reversibility and cyclability demands the development of new combinations of alloys and catalysts. Combinatorial synthesis, coupled with high-throughput screening methodologies, is thus seen as one of the most efficient strategies for the discovery of new effective hydrogen storing materials [2–9].

On the other hand, reduction of the systems to the nanoscale by preparing nanostructured or nanocomposite bulk or thin films, has demonstrated improved hydrogen sorption and desorption kinetics [10–12]. In thin films hydrogenation/dehydrogenation is not significantly kinetically limited because of the short diffusion paths involved, and furthermore lower reaction temperatures can be used for testing effective hydrogenation on new systems. Therefore, the synergy of nanoscale phenomena in thin films with high throughput screening techniques is expected to foster the discovery of new hydrogen storing material as well as to optimize its associated reaction promoter/catalyst. Besides, although thin films presents limited industrial applications as storing systems, due to the reduced amount of stored hydrogen, novel applications such as hydrogen sensors and switchable mirrors have already been proposed [13–17]. Another advantage of introducing a thin film approach to the research of new hydrides arises from the fact that metastable or amorphous phases, inaccessible by other techniques, can be easily synthesized and studied.

In the last years, optical methodologies have appeared as one of the most appropriate combinatorial techniques due to their apparent simplicity and low cost, and are presently exploited to characterize the hydrogen absorption/desorption of metallic thin films libraries [2–8]. Among the proposed techniques, as metal hydrides generally shift from metal to semiconducting behavior during their hydrogenation, and thus from lower to higher emissivities, infrared thermography has been successfully used for *in situ* hydrogen sorption studies in binary [6–8] or ternary magnesium-based compounds [2,3].

Two main strategies are generally developed to improve the properties of magnesium hydrides. The first one consists of adding catalysts elements such as Pd, Ti, Fe to accelerate the reaction kinetics; the second one is based on the destabilization of the hydride by forming intermediate alloys that can be reversibly hydrogenated, by adding elements like Cu, Si, Al. For instance, aluminum has been found to destabilize MgH_2, reducing the enthalpy down to 28 kJ/mol H_2 by forming Mg_2Al_3 or $Mg_{17}Al_{12}$ alloys [18–20].

* Corresponding author. Tel.: +34 935811481; fax: +34 935812155.
E-mail address: gemma.garcia@uab.cat (G. Garcia).
[1] Present address: Institute of Metallic Materials, IFW, Helmholtzstraße 20, D-01069 Dresden, Germany.

0920-5861/$ – see front matter © 2010 Elsevier B.V. All rights reserved.
doi:10.1016/j.cattod.2010.10.002

In the present article, we study the suitability of an infrared imaging methodology for analyzing the hydrogen sorption and desorption of magnesium-based thin film libraries. To study the performances and limitations of the technique, we prepared and characterized two types of libraries, one based on discrete multilayered samples prepared using sets of moving shadow masks, and the second based on the compositional-spread methodology. The discrete libraries were prepared by sequential *e*-beam evaporation of pure aluminum and magnesium films, while the composition-spread libraries were grown by co-sputtering of Mg, Fe and Cu.

To our knowledge a quaternary alloy formed by Mg–Fe–Cu–H has not been reported yet. Nevertheless, the individual effects of Fe and Cu on the Mg/MgH_2 have already been described. The Mg–Fe–H forms the Mg_2FeH_6 ternary alloy with a theoretical storing capacity of 5.47 wt.% and an enthalpy of formation close to 77 kJ/kg [21]. Due to its high stability, this alloy desorbs at temperatures above 300 °C in 1 bar H_2. Other authors have analyzed the effect of adding Fe to the MgH_2 system and found that its presence decreased the dehydrogenation temperature [22–25]. In the Mg–Cu system, no ternary Mg–Cu–H compound has been identified yet, but as in the case of Fe, the addition of Cu to MgH_2 has been theoretically found to destabilize MgH_2 through formation of Mg–Cu intermetallic alloys: $2MgH_2 + Cu \leftrightarrow Mg_2Cu$; and to decrease the desorption temperature due to the decrease of the unit cell volume when Cu atoms are incorporated in the MgH_2 structure [26–28].

Infrared imaging detects changes in the apparent temperature of the samples that may be correlated to emissivity changes or to real temperature variations associated to an energetic process occurring in the sample. In conventional bulk samples, hydrogenation and dehydrogenation reactions are accompanied by changes in temperature, due to the large enthalpies of reaction (ΔH), which can be detected by thermography. However, in thin films, especially when deposited over highly conducting substrates such as Si or sapphire, the temperature variation induced by the enthalpy of the transformation is much lower than the apparent temperature shift due to changes of the surface emissivity. Therefore, the screening of the emissivity changes can be a more effective and precise methodology to analyze phase transformation in thin films. As metal hydrides generally show a shift from metal to semiconducting behavior during hydrogenation, and thus from lower to higher emissivities, infrared imaging has been used for *in situ* hydrogen sorption and desorption studies, as presented by Olk et al. [2,3] in the multicompositional Mg–Ni–Fe system, and more recently by Guerin et al. [6] and Oguchi et al. [7,8] both in the MgNi system. Compared to those previous infrared imaging reported works our differential data analysis and specific treatment; permit the determination of reaction temperatures for any composition of the library generating reaction temperature maps. Using this tool, the effects of adding Al, Fe and Cu on the sorption and desorption temperatures of magnesium based films are analyzed and discussed.

2. Experimental

Hydrogenation treatments and *in situ* thermographic characterization were performed in a high vacuum chamber where pressure can vary from vacuum up to 1.0 bar with pure or mixed He and H_2 atmosphere and from room temperature to 300 °C. An infrared camera, Jenoptik IR-TCM 384, is mounted over a ZnSe chamber view-port to record the IR images of the sample during thermal treatments. Before any experiment the chamber is purged three times with helium to minimize the presence of oxygen and moisture. The IR image acquisition and thermal treatment are lumped to assign a temperature/time correspondence during constant heating and isothermal treatments. Irbis 3.0 software provided by JENOPTIK allowed visualization and basic features analyses of IR images such as determination of single point's apparent temperature (T_a), average temperature over a determined surface and temperature profiles from any path. Nevertheless, for the study of time/temperature evolution, where sequences of images have to be analyzed, special home-made software has been developed to determine the reaction temperature for each image pixel i.e. for all the compositions of the library, generating reaction temperature maps for several studied hydrogen partial pressures.

To minimize systematic errors due to external factors affecting the IR data, an IR image is collected at room temperature before any treatment and the extracted data matrix used as background to be subtracted to the subsequent files. Furthermore, a non-reacting sample is imaged in parallel, to work in the so-called differential mode. Generally, the stainless steel heater surface (which is not expected to react with hydrogen atmosphere at least in the analyzed temperature ranges) is recorded in the same IR frame together with the sample and its apparent temperature (T_h) evolution is used as the reference to be subtracted in the so-called differential mode. This methodology permits discriminating variations in T_a (apparent temperature of the sample) due to heating or cooling treatments from those really corresponding to a hydrogen absorption or desorption reactions or to any other chemical reaction producing accompanied by an emissivity change.

Table 1
Description of the library showing the nominal total and individual layer thicknesses of the Mg and Al film deposited sequentially for the 16 frames of the discrete library. The frames composition (at.% magnesium) were determined by EDS.

Al	Mg			
	75 nm 3 × 25 nm	110 nm 3 × 37 nm	150 nm 3 × 50 nm	300 nm 3 × 100 nm
0 nm	100	100	100	100
150 nm 2 × 75 × nm	30	39	46	62
175 nm 2 × 87 nm	26	34	42	55
200 nm 2 × 100 nm	22	27	37	46

3. Results and discussion

3.1. IR thermography on binary MgAl libraries

Geometrically defined thin films libraries of Mg and Al were prepared using the sequential *e*-beam evaporation methodology described elsewhere [9]. By using moving shadow masks coupled to a sequential deposition of aluminum and magnesium single layers, we prepared libraries with 16 discrete frames, where each frame is formed by two Al layers intercalated between three Mg layers. Single layers of magnesium varied from 25 to 100 nm, thus total thickness ranged from 75 to 300 nm. On the other side intercalated aluminum varied from 0 to 100 nm giving rise to total Al thickness ranging from 0 to 200 nm, as shown in Table 1. The different Mg and Al thicknesses, give rise to library compositions ranging from 22 to 100 at.% of magnesium. Notice that the first raw of the library was formed by pure magnesium films to study the effect of its thickness on the reaction kinetics. Also the columns of the library were defined in order to allow the analysis of the effect on the intercalated aluminum thickness for similar magnesium amount. Mention that the Mg/Al multilayers were sandwiched between two layers of Pd (15 nm) and Fe (10 nm), forming the following heterostructure: Pd/Fe/Mg/Al/Mg/Al/Mg/Fe/Pd. The Pd was added to ensure fast hydrogen dissociation and diffusion rates, as well as to avoid oxidation of magnesium, while the iron role was added to prevent the formation of MgPd alloys such as Mg_6Pd. The nominal thickness sequences and the composition estimated by energy dis-

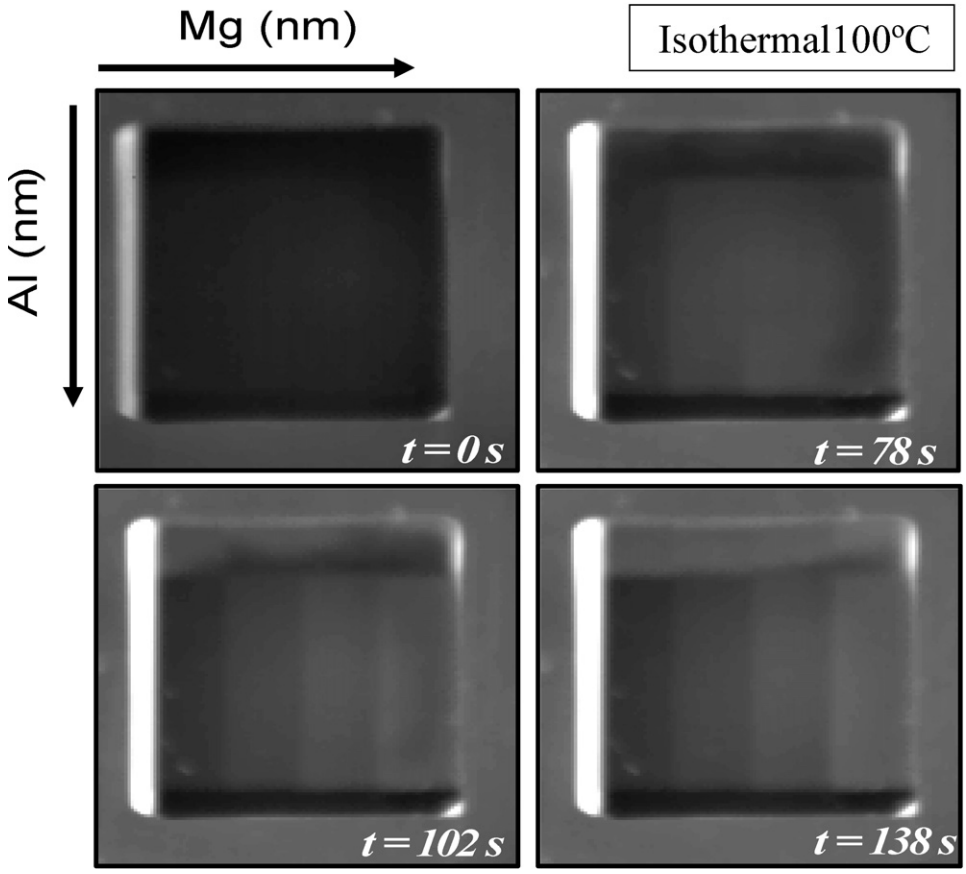

Fig. 1. Thermal images of the MgAl library during isothermal treatment performed at 100 °C and 520 mbar H_2 as a function of time.

persive X-ray spectroscopy (EDS) for each frame are summarized in Table 1.

The IR screening of such libraries was performed using the VarioCAM thermographic camera during an isothermal treatment. The library was heated up to 100 °C in pure helium to stabilize the temperature prior to imaging. After few minutes, we start recording an image every 6 s and introduce hydrogen in the chamber until the hydrogen partial pressure (P_{H_2}) reaches 500 mbar. Fig. 1 shows a sequence of the IR images acquired during this hydrogenation process. At time $t = 0$, where no hydrogen has been yet introduced into the chamber, the library looks totally dark, as expected for a metallic material; in comparison the residual non-coated silicon substrate area, that can be seen in the left lateral of the library, presents a shiny aspect which is associated to its semiconducting-like emissivity. After introducing the hydrogen, the dark frames became clear and the boundaries between the library's frames started to appear. Although no clear conclusions could be extracted from the visual inspection, the brightness evolution of the first raw indicated that as expected the thinnest Mg showed the faster reaction times to reach the shiny aspect associated to the hydrogenated state. Furthermore, if we compare the aspect evolution of this pure magnesium raw with the aluminum intercalated ones we can see that in general the aluminum "doped" frames turn shiny more rapidly; indicating that the aluminum could act as a promoter of the hydrogenation reaction.

To precisely analyze the hydrogenation reaction kinetics, we perform the image treatments described previously to determine the differential apparent temperature evolution with time, as shown in Fig. 2. As an example of the observed behavior, we plot the $T_a - T_h$ evolution of three different thicknesses pure magnesium frames (first raw of the library) as well as that of several intercalated aluminum thickness samples but with similar total magnesium amount – 300 nm thickness (corresponding to the fourth column of the library).

Immediately after introducing H_2 inside the chamber, an overshoot in ($T_a - T_h$) was observed corresponding to a real temperature increase caused by the introduction of a highly thermal conducting gas. After around 50 s, $T_a - T_h$ returns to its initial value and then increase up to a certain stabilized value that depends on the frame. The reaction time can thus be extracted from those representations as point where the curve slope becomes almost null, as schematized in Fig. 2 with arrows. As expected from the previ-

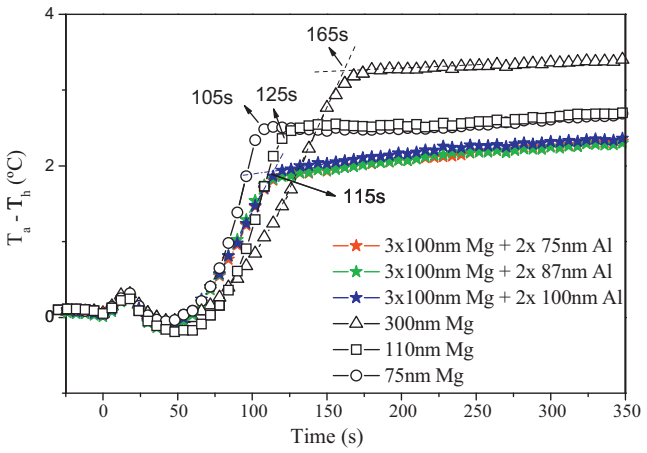

Fig. 2. Evolution of the differential apparent temperature ($T_a - T_h$) as a function of time during an isothermal treatment at 100 °C for selected members of the library.

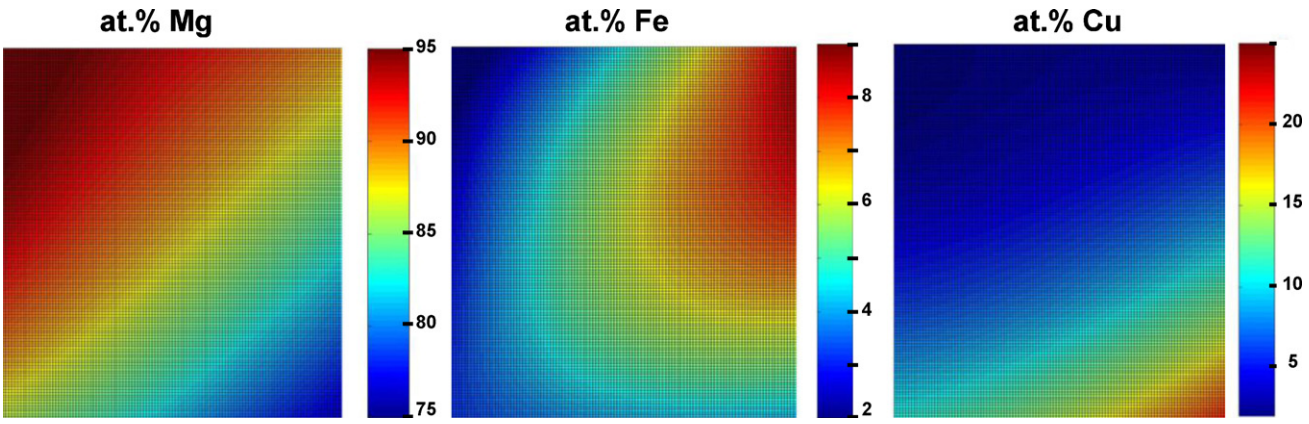

Fig. 3. Composition maps of the MgFeCu libraries, showing the area distribution of the Mg, Fe and Cu by EDS. The color bars indicate the composition scale in at.%. (For interpretation of the references to color in this figure legend, the reader is referred to the web version of the article.)

ous visual observation, the reaction time of pure magnesium film increases with increasing thickness from 105, 125 and 165 s for 75, 110 and 300 nm, respectively. Also, the final absolute value of the stabilized ($T_a - T_h$) seems to depend on thickness, as 300 nm films reach higher value than that of 75 or 110 nm samples, which are both quite similar. On the contrary, samples with different intercalated aluminum layers but identical magnesium amount exhibit a striking behavior. The plotted representative cases, corresponding to similar 300 nm magnesium (3 nm × 100 nm) but with different intercalated aluminum thickness (2 nm × 75 nm, 2 nm × 87 nm and 2 nm × 100 nm), showed a similar reaction time, 115 s, and identical final plateau value.

This reaction time is almost equivalent to that of the 110 nm pure Mg although the final $T_a - T_h$ value is smaller than that observed for any studied magnesium thickness. Those results seem to indicate that the reaction time extracted for aluminum intercalated frames could in fact be only associated to the hydrogenation reaction time of the upper single Mg layer. On the contrary to the reaction time which appears to be independent of the presence of intercalated aluminum, the final $T_a - T_h$ seems to be effectively influenced by the buried aluminum although no variation has been observed as a function of the aluminum thickness. This phenomenon can be explained by the fact that aluminum do not hydrogenate and remains in a metallic state being thus opaque to any radiation that originates from deeper buried magnesium layers. It is therefore difficult to correlate the final $T_a - T_h$ values to any hydrogen storage capacity, at least using multilayered systems. A deeper theoretical analysis considering the dielectric function of the various materials in stack geometry is under way.

3.2. IR thermography of ternary MgFeCu libraries

In view of the limitations arising from the multilayered thin film samples thermographic analysis, we prepare and characterize co-deposited thin films libraries, where the intimated mixing of components will allow us to characterize the effect of added elements as reaction promoter avoiding geometrical effects. Ternary Mg–Fe–Cu libraries were thus deposited using the co-sputtering technique with Mg and Cu targets facing each other and Fe gun located at 90°. The depositions were performed at room temperature and 2×10^{-2} mbar of Ar (99.999% purity) on Si substrates (4 cm × 6 cm). A thin SiO_2 layer (nominal thickness 130 nm) was grown previously to avoid direct contact of Mg with Si enabling the formation of Mg_2Si. As in the previous case, the libraries were coated with 10 nm of Pd to avoid oxidation of the samples and also to catalyze the dissociation of the hydrogen molecule at the surface. The library thickness was 60 ± 5 nm and the overall compositional maps of Mg, Fe and Cu shown in Fig. 3 were estimated by interpolation with a second order polynomial of the local composition measured by EDS on a 4 × 4 equidistant point's matrix. As expected the compositional gradients follow the location of the target guns in the equipment. The Mg-rich areas of the library were found in the left upper part ranging from 75 to 95 at.%, while Cu-rich zone was located just at the opposite corner ranging from 3 to 25 at.%. The iron-rich region was located in the upper right side and varied from 2 to 9 at.%. It is worth noting, that in order to avoid cycling of an unknown system, we prepared 4 identical libraries to perform individual and unique IR imaging during hydrogen sorption at each precise partial pressure. The 4 libraries presented minimal composition differences in the range of EDS accuracy (when performed on thin film) due to slight misalignments of the rotational axes of the wafer during introduction in the main chamber.

The four libraries were previously hydrogenated in 950 mbar of pure H_2 during 8 h at 100 °C and the dehydrogenation processes were carried out at four different hydrogen partial pressures: $P_{H_2} = 0$ mbar (pure He), $P_{H_2} = 19$ mbar, $P_{H_2} = 52$ mbar and $P_{H_2} = 137$ mbar. To ensure a similar thermal conduction in the reaction chamber the total working pressure was set around atmospheric pressure by filling the chamber with helium. The dehydrogenation process was screened acquiring an image every 150 s during heating ramps at 10 K/h (one image each 0.4 K). As described in former section, from the $T_a - T_h$ evolution, in that case as a function of real temperature, we determined $T_{desorption}$ (or $T_{dehydrogenation}$) for each image pixel, i.e. every composition of the library, as the temperature where an abrupt change in slope is observed; resulting in the $T_{desorption}$ maps shown in Fig. 4. As can be seen in the figure for the four studied P_{H_2}, black areas appear in the map, mainly corresponding to the non-coated areas beneath the substrate holding system but also to some parts of the libraries where no reliable desorption temperature could be extracted. Those areas of the libraries were thus ignored for the present study. Mentioning that those "non-reacting" areas correspond to the richest Cu parts with more than 15 at.% Cu (and around at. 2 at.% Fe) of the libraries. The present dehydrogenation study and discussion will thus be limited to lower Cu compositions. The $T_{desorption}$ maps showed that whenever P_{H_2}, the highest desorption temperatures were always found in the Fe richest parts of the library, while for the poor Fe areas, desorption temperatures decreased almost following the Mg–Cu compositional gradient line, i.e. the lowest temperatures were found in the richest Cu-analyzed areas. Also, as expected, desorption was promoted by reducing hydrogen partial pressure P_{H_2} and thus globally dehydrogenation temperatures increased by increasing the hydrogen pressure inside the chamber. The extracted $T_{desorption}$ values ranged between 80 and 130 °C,

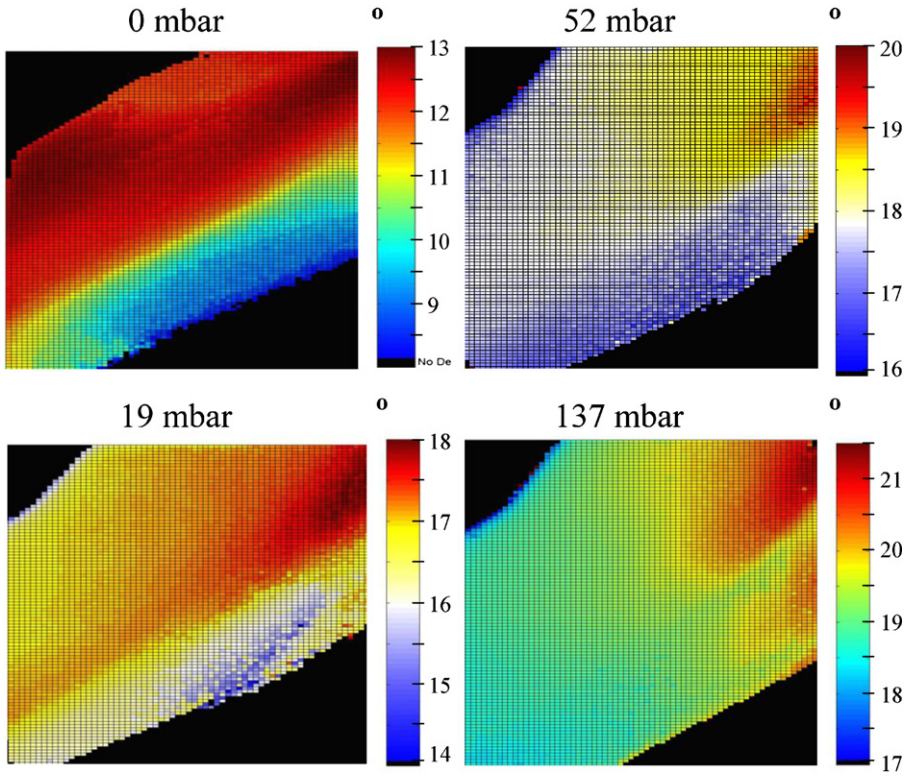

Fig. 4. $T_{dehydrogenation}$ maps over of the MgFeCu libraries measured by thermography at several P_{H_2} partial pressures: 0 mbar, 19 mbar, 52 mbar and 137 mbar.

between 140 and 180 °C, between 60 and 200 °C and between 170 and 215 °C for $P_{H_2} = 0$ mbar, 19 mbar, 52 mbar and 137 mbar, respectively.

If we plot the variation of $T_{desorption}$ as a function of the Cu content fixing the Mg and Fe amounts, as shown in Fig. 5, we see that at least for lower hydrogen partial pressure, introducing copper up to 14 at.% clearly reduced the desorption temperatures from 130 °C to 95 °C for pure helium atmosphere, and from 160 °C to 150 °C for 19 mbar P_{H_2}. For higher P_{H_2}, the effect of the copper was reduced and probably larger amount should be added to the system to observe any improvement in hydrogen desorption.

Similarly, if we plot the evolution of $T_{desorption}$ as a function of the Fe content for a fixed amount of Mg and Cu, as shown in Fig. 6, we can clearly appreciate that Fe do not seems to have any positive influence as a slight increase of the desorption temperature was observed when increasing P_{H_2}. On the contrary to copper, iron unaffected or slightly worsen the desorption properties of the system.

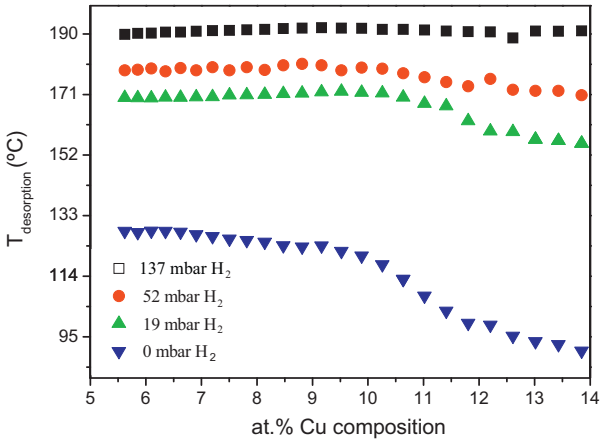

Fig. 5. Variation of $T_{dehydrogenation}$ as a function of Cu content for a fixed composition of Fe and Mg (Fe 3 at.% and Mg 82–91 at.%).

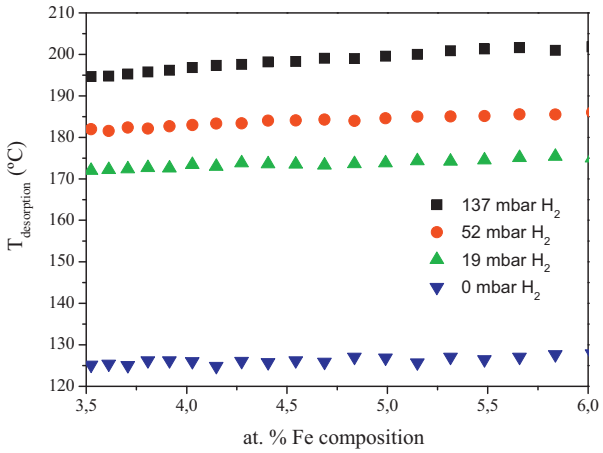

Fig. 6. Variation of $T_{dehydrogenation}$ as a function of Fe content for a fixed composition of Cu and Mg composition (Cu 6 at.%, Mg 87.5–90.5 at.%).

It is worth noting that separately, both elements, Cu and Fe, have been found to catalyze the hydrogenation desorption [22–25] of Mg, which is not the case for Fe in the present study. As Mg_2FeH_6 is not expected to be formed in the studied temperature and pressure conditions, we cannot assign the observed slight $T_{desorption}$ increase to the formation of such ternary hydride.

4. Conclusions

In this paper we show the potentialities and limitations of the infrared thermography as a tool to analyze the hydrogen storage properties in magnesium based thin films libraries, as well as the

role of added elements such as Al, Cu or Fe as promoter of the hydrogenation/dehydrogenation reaction. Nevertheless, we have found that co-deposited libraries suits better to the IR imaging than multilayered systems, as information from the whole volume can be characterized. For MgFeCu the data treatment permit the determination of desorption temperature maps for every sample composition, allowing for the study of possible catalysts effect enhancing the hydrogen desorption. In the present case, Cu seems to act as a catalyst for the dehydrogenation process while Fe presented an unexpected negative effect. Clearly, improvements also have to be performed to the experimental conditions and procedure in order to ensure thermodynamic equilibrium during the experiments that will permit the determination of the reaction enthalpies.

Acknowledgements

This work has been partially supported by MICINN -MAT2007-61521, the Generalitat de Catalunya through SGR2009-01225 and the SOST-CENIT project.

References

[1] B. Bogdanovich, M. Schvickardi, J. Alloys Compd. 235–254 (1997) 1–9.
[2] C.H. Olk, G.G. Tibbetts, D. Simon, J.J. Moleski, J. Appl. Phys. 94 (1) (2003) 720.
[3] C.H. Olk, Meas. Sci. Technol. 16 (2005) 14–20.
[4] B. Dam, R. Gremaud, C. Broedersz, R. Griessen, Scripta Mater. 56 (10) (2007) 853.
[5] R. Gremaud, C.P. Broedersz, D.M. Borsa, A. Borgschulte, P. Mauron, H. Schreuders, J.H. Rector, B. Dam, R. Griessen, Adv. Mater. 19 (19) (2007) 2813.
[6] S. Guerin, B.E. Hayden, D.C.A. Smith, J. Comb. Chem. 10 (2008) 37–43.
[7] H. Oguchi, J. Hattrick-Simpers, I. Takeuchi, E.J. Heilweil, L.A. Bendresky, Rev. Sci. Instrum. 80 (2009) 073707.
[8] H. Oguchi, E.J. Heilweil, D. Josell, L.A. Bendersky, J. Alloys Compd. 477 (1–2) (2009) 8–15.
[9] G. Garcia, R. Domènech-Ferrer, F. Pi, J. Santiso, J. Rodríguez-Viejo, J. Comb. Chem. 9 (2007) 230–236.
[10] A. Zaluska, L. Zaluski, J.O. Ström–Olsen, J. Alloys Compd. 288 (1–2) (1999) 217–225.
[11] A. Zaluska, L. Zaluski, J.O. Ström-Olsen, Appl. Phys. A 72 (2001) 157–165.
[12] G. Liang, J. Huot, S. Boily, A. Van Neste, R. Schulz, J. Alloys Compd. 292 (1–2) (1999) 247–252.
[13] B. Farangis, P. Nachimuthu, T.J. Richardson, J.L. Slack, B.K. Meyer, R.C.C. Perera, M.D. Rubin, Solid State Ionics 165 (1–4) (2003) 309–314.
[14] S. Bao, K. Tajima, Y. Yamada, M. Okada, K. Yoshimura, Appl. Phys. A 87 (2007) 621–624.
[15] A. Baldi, D.M. Borsa, H. Schreuders, J.H. Rector, T. Atmakidis, M. Bakker, H.A. Zondag, W.G.J. van Helden, B. Dam, R. Griessen, Int. J. Hydrogen Energy 33 (12) (2008) 3188–3192.
[16] D.M. Borsa, A. Baldi, M. Pasturel, H. Schreuders, B. Dam, R. Griessen, P. Vermeulen, P.H.L. Notten, Appl. Phys. Lett. 88 (2006) 241910.
[17] Y. Yamada, S. Bao, K. Tajima, M. Okada, K. Yoshimura, A. Roos, Sol. Energy Mater. Sol. Cells 92 (12) (2008).
[18] R. Gremaud, A. Borgschulte, C. Chacon, J.L.M. van Mechelen, H. Schreuders, A. Züttel, B. Hjörvarsson, B. Dam, R. Griessen, Appl. Phys. A 84 (2006) 77–85.
[19] A. Andreasen, Int. J. Hydrogen Energy 33 (2008) 7489–7497.
[20] R. Domènech-Ferrer, M.G. Sridharan, G. Garcia, F. Pi, J. Rodríguez-Viejo, J. Power Sources 169 (2007) 117–122.
[21] A. Reiser, B. Bogdanovic, K. Schlichte, Int. J. Hydrogen Energy 25 (2000) 425–430.
[22] B. Bogdanović, A. Reiser, K. Schlichte, B. Spliethoff, B. Tesche, J. Alloys Compd. 345 (2002) 77–89.
[23] M.D. Riktor, S. Deledda, HerrichF M., O. Gutfleisch, H. Fjellvåg, B.C. Hauback, Mater. Sci. Eng. B 158 (1–3) (2009) 19–25.
[24] R.A. Varin, S. Li, Ch. Chiu, L. Guo, O. Morozova, T. Khomenko, Z. Wronski, J. Alloys Compd. 404–406 (2005) 494.
[25] C.X. Shang, M. Bououdina, Y. Song, Z.X. Guo, Int. J. Hydrogen Energy 29 (2004) 73.
[26] J.J. Reilly, R.H. Wiswall, Inorg. Chem. 6 (1967) 2220–2223.
[27] Q. Li, J. Liu, K.C. Chou, G.W. Lin, K.D. Xu, J. Alloys Compd. 466 (1–2) (2008) 146–152.
[28] N. Takeichi, K. Tanaka, H. Tanaka, T.T. Ueda, Y. Kamiya, M. Tsukahara, H. Miyamura, S. Kikuchi, J. Alloys Compd. 446–447 (2007) 543.